

# IM-IAD: Industrial Image Anomaly Detection Benchmark in Manufacturing

Guoyang Xie<sup>1</sup>, *Member, IEEE*, Jinbao Wang<sup>1</sup>, *Member, IEEE*, Jiaqi Liu<sup>1</sup>, Jiayi Lyu, Yong Liu, Chengjie Wang, Feng Zheng\*, *Member, IEEE*, and Yaochu Jin\*, *Fellow, IEEE*

**Abstract**—Image anomaly detection (IAD) is an urgent issue that needs to be addressed in modern industrial manufacturing (IM). Recently, many advanced algorithms have been released, but their performance varies greatly due to non-uniformed settings. That is, researchers find it difficult to analyze because they are designed for different or specific cases in IM. To eliminate this problem, we first propose a uniform IAD setting to systematically assess the effectiveness of these algorithms, mainly considering three aspects of supervision level (unsupervised, fully supervised), learning paradigm (few-shot, continual, noisy label), and efficiency (memory usage, inference speed). Then, we skillfully construct a comprehensive image anomaly detection benchmark (IM-IAD), which includes 19 algorithms on 7 major datasets with the same setting. Our extensive experiments (17,017 total) provide new insights into the redesign or selection of the IAD algorithm under uniform conditions. Importantly, the proposed IM-IAD presents feasible challenges and future directions for further work. We believe that this work can have a significant impact on the IAD field. To ensure reproducibility and accessibility, our source codes are uploaded to the website: <https://github.com/M-3LAB/open-iad>.

## I. INTRODUCTION

There is a strong need to come up with a uniform industrial setting that is highly important to fill the gap and bring new capabilities of image anomaly detection (IAD) algorithms to the factory floor. IAD is an important computer vision task for industrial manufacturing (IM) applications [57], [75], [76], such as industrial products surface anomaly detection [84], [32], textile defect detection [72], [41], and food inspection [8], [92]. Due to the gap between academia and industry, only a few IAD algorithms are used in real manufacturing. In the computer vision community, there is a primary focus on unsupervised methods, but there is little analysis of the

Guoyang Xie is with the Department of Computer Science and Engineering, Southern University of Science and Technology, Shenzhen 518055, China and is also with the Department of Computer Science, University of Surrey, Guildford GU2 7YX, United Kingdom (e-mail: guoyang.xie@ieee.org)

Jinbao Wang, Jiaqi Liu and Feng Zheng are with the Department of Computer Science and Engineering, Southern University of Science and Technology, Shenzhen 518055, China (e-mail: wangjb@ieee.org; liujq32021@mail.sustech.edu.cn; f.zheng@ieee.org)

Yong Liu and Chengjie Wang are with Tencent Youtu Lab, Shenzhen 518040, China (e-mail: chaosliu@tencent.com; jasoncjwang@tencent.com)

Jiayi Lyu is with the School of Engineering Science, University of Chinese Academy of Sciences, Beijing, China (e-mail: lyujiayi21@mails.ucas.ac.cn)

Yaochu Jin is with the School of Engineering, Westlake University, Hangzhou 310030, China and also with the Department of Computer Science and Engineering, University of Surrey, Guildford GU2 7YX, United Kingdom (e-mail: jinyaochu@westlake.edu.cn)

<sup>1</sup>Contributed equally.

\*Co-corresponding authors.

TABLE I  
THE COMPARISON WITH IAD AND RELATED BENCHMARKS IN TERMS OF DATASET, LEARNING PARADIGM, ALGORITHM AND METRIC.

Category	Classification / Attribute		Mark		
Work	–		[93]	[28]	IM-IAD
Dataset	MVTec AD [4], [2]		✓	✓	✓
	MVTec LOCO-AD [3]		\	\	✓
	BTAD [52]		\	\	✓
	MPDD [33]		\	\	✓
	MTD [32]		\	\	✓
	VisA [94]		\	\	✓
	DAGM [18]		\	\	✓
Paradigm	Unsupervised		✓	✓	✓
	Fully Supervised		\	\	✓
	Few-Shot		\	\	✓
	Noisy Label		\	✓	✓
	Continual		\	\	✓
Algorithm	Feature Embedding	Normalizing Flow	✓	\	✓
		Memory Bank	✓	\	✓
		Teacher-Student	✓	\	✓
		One-Class Classification	✓	\	✓
	Reconstruction	External Data	✓	\	✓
		Internal Data	✓	\	✓
			✓	\	✓
Metric	AUROC	Image- and Pixel-Level	✓	\	✓
	AUPR/AP	Image- and Pixel-Level	✓	\	✓
	PRO	Pixel-Level	\	\	✓
	SPRO	Pixel-Level	\	\	✓
	FM	Image- and Pixel-Level	\	\	✓
	Efficiency	Inference Speed	✓	\	✓
Uniform	–		\	\	✓

industry's demands. Because of this, it is important and urgent to build a uniform setting<sup>3</sup> for IM.

The proposed setting, IM-IAD, summarized in this paper, such as unsupervised, fully supervised, few shot, continual learning, and noisy label, is more suitable for assessing the performance of IAD methods in real industrial production. Previous work has made some progress on certain aspects, such as DRA [25], Softpach [35] and DNE [45]. However, most solutions proposed these work cannot meet the requirements of realistic IM applications. For instance, Huang *et al.* [31] employ meta-learning as a few-shot IAD. Due to complicated settings, it is impossible to migrate to the new product during the manufacturing changeover scenario, and detection accuracy cannot be guaranteed. In terms of the training speed, when a large amount of data is utilized for

<sup>3</sup>Setting means the configuration for various learning paradigms.

training, the training progress for new goods is slowed down in the actual production line. There are few methods that focus on the efficiency of models [71], [24]. Many existing methods tend to prioritize higher accuracy. As a result, they often use larger backbone networks. This can lead to a neglect of the detection efficiency. SimpleNet [49] is significantly faster than previous methods, but its performance can be quite unstable during training due to the use of a GAN-like structure. EfficientAD [1] employs a fully convolutional structure to accelerate anomaly detection, but this structure also achieves high accuracy only for certain types of data. Meanwhile, other methods still mainly focus on research guided by detection accuracy.

For this reason, our IM-IAD setting aims to push the boundaries of IAD methods in practical scenarios, while previous benchmarks cannot accurately reflect the needs of IM. There are two notable works [93], [28] that take effort to benchmark IAD algorithms. The distinction between IM-IAD and previous benchmarks lies in the following aspects. Firstly, previous studies mainly concentrate on benchmarking IAD methods based on the level of supervision [28]. However, they [93], [28] ignore realistic IM scenarios, *i.e.*, continual learning, few-shot learning, and noisy label. It is crucial because most IAD algorithms are not suitable for production lines. Our proposed IM-IAD setting makes researchers aware of the gap between academia and industry and offers deeper insights into future improvements. Secondly, ADBench [28] focuses primarily on tabular and graph-structured data, but not image data, and no IAD algorithms have been evaluated on the benchmark. Even for [93], they only assess unsupervised IAD algorithms on two datasets. However, we constructed a comprehensive benchmark, IM-IAD with 7 industrial datasets and 19 algorithms, shown in Table II.

In this paper, we address the above issues in IAD through extensive experiments. The **key takeaways** are preferably presented as follows. 1) Regarding accuracy, memory usage, and inference speed, none of the benchmarked unsupervised IAD algorithms is statistically better than others, highlighting the importance of selecting types of anomaly. 2) The long-distance attention mechanism shows great potential in logical IAD, possibly due to its global feature extraction abilities. 3) Fully supervised methods have demonstrated superior performance compared to unsupervised IAD. This can be attributed to the fact that the incorporation of labeled anomalies into the training process significantly enhances IAD capabilities. 4) With merely 4 augmented (rotated) data, feature embedding-based few-shot IAD algorithms can achieve the performance 95% of vanilla IAD, revealing the necessity of data characteristics. 5) Importance reweighting successfully improves the resilience of IAD algorithms, even though the noise ratio is larger than 10%. 6) Memory bank can be seamlessly incorporated into advanced IAD algorithms, considerably enhancing their capacity to resist catastrophic forgetting.

The main contributions are summarized as follows.

- We extract scientific problems from the manufacturing process and present a standardized and unified setting to bridge the gap between academic research and industrial practices in the identification of image anomalies.

- We examine 16 IAD methods on 7 benchmark datasets, resulting in a total of 17,017 instances. Additionally, we present a plug-and-play and modular implementation for fair IAD evaluation, which greatly benefits the future development of IAD algorithms.
- By analyzing the requirements of research and industrial manufacturing processes, we examine four key aspects of IAD algorithms for comparison: the changeover-based few-shot representational abilities; the trade-off between accuracy and efficiency; the catastrophic forgetting phenomenon; and the robustness of the algorithm in the presence of noise labeling. Based on these aspects, we offer deep insights and suggest future directions.

The rest of this paper is organized as follows. Sec. II presents a literature review on IAD methods and mainstream learning paradigms. Sec. III provides our proposed uniform setting in IM-IAD. In detail, we give comprehensive experimental evaluations in Sec. IV and discuss the advanced model performance in different settings. Finally, Sec. V draws the conclusion of our work.

## II. RELATED WORK

This section has reviewed the current IAD methods concluded in Table I with five settings that are visualized in Fig. 1 and are defined in Sec. III-A.

**Unsupervised IAD.** There are two main areas of research on unsupervised IAD [46], namely feature embedding-based methods [5], [61], [15], and reconstruction-based methods [81], [88]. Specifically, feature embedding-based approaches can be divided into four categories, including teacher-student [5], normalizing flow [61], memory bank [15], and one-class classification [68]. The most typical methods are teacher-student models and memory bank-based models. As for teacher-student models, the teacher model extracts the features of normal samples and distills the knowledge to the student model during the training phase. Regarding abnormal images, the features extracted by the teacher network may deviate from those of the student network during the test phase. Thus, the basic rule for finding anomalies is that the teacher-student network has different features. Regarding memory bank-based approaches [15], [44], [37], the models capture the features of normal images and store them in a feature memory bank. During the testing phase, the feature of the test sample queries the memory bank for the feature points of  $k$ -nearest neighborhoods. If the distance between the test feature and the closest feature points of neighborhoods exceeds a specific threshold, the test sample is categorized as anomalous. However, both of them heavily depend on the power of the teacher network or the size of memory bank, which may limit the ability of generalization in real-world industry.

**Fully supervised IAD.** Regarding the setting, the distinction between unsupervised IAD and fully supervised IAD [43], [14], [25] is the use of abnormal images for training. Fully-supervised IAD methods [73], [54] focus on how to efficiently employ a small number of abnormal samples to distinguish the features of abnormalities from those of normal samples. Nevertheless, the performance of some fully supervised IAD

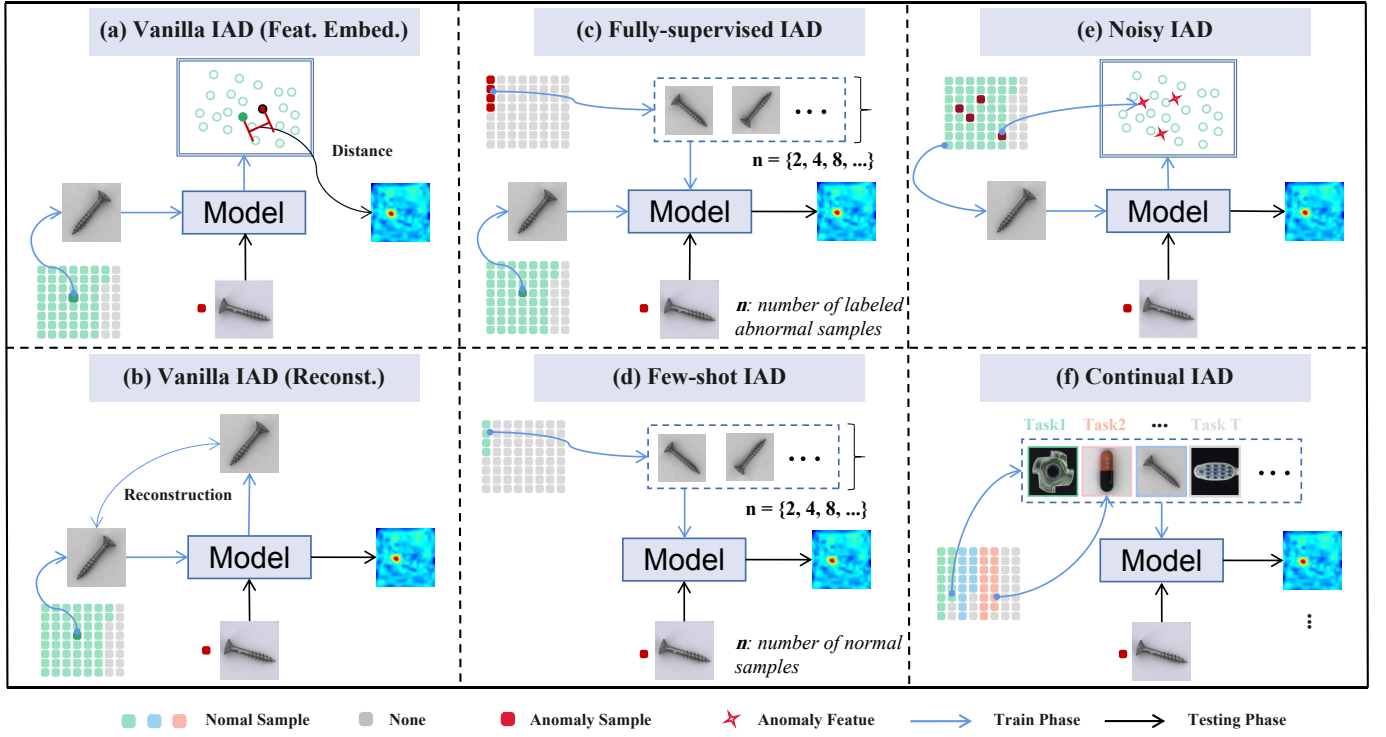


Fig. 1. Illustration of the IM-IAD setting. The vanilla unsupervised IAD methods only using normal samples can be divided into two categories, namely feature embedding-based and reconstruction-based methods. (a) Feature embedding-based methods find the difference between the test samples and normal samples at the feature level, while (b) reconstruction-based methods compare the difference between the input image and the reconstructed image to determine whether it is abnormal or not. For fully supervised methods (c), they use limited abnormal samples with annotations to improve the model performance. The few-shot setting (d) uses only a small number of normal samples for training. The noisy setting (e) mixes abnormal samples in the training set and evaluates the robustness of the model. The continual setting (f) trains on each task in turn and evaluates how much the model forgets past tasks.

approaches is inferior to that of unsupervised methods for identifying anomalies. There is still room for improvement regarding the use of data from abnormal samples.

**Few-shot IAD.** The few-shot (including zero-shot) IAD is very promising because it can greatly reduce the demand for data volume. However, it is still in the early stages of research, and existing IAD methods are usually not specialized in this setting. PatchCore [77] designs the efficient visual isometric invariant feature for a few-shot task, which can perform fast training and significantly improve the ability to discriminate anomalies using a few samples. Furthermore, by leveraging diverse multi-modal prior knowledge of foundation models (like Segment Anything [38]) for anomalies, Cao *et al.* [9] achieve state-of-the-art performance on several benchmarks in the zero-shot setting. Due to the real needs of industrial scenarios, few-shot learning remains a future research focus in the field of anomaly detection.

**Noisy IAD.** Noisy learning is a classic problem for anomaly detection [56], [111]. However, in the field of IAD, training with noisy data is an inevitable problem in real practice. Such noise usually comes from inherent data shifts or human misjudgment. To address this problem, SoftPatch [35] is the first to efficiently denoise data at the patch level in an unsupervised manner. By contrast, other methods rarely discuss this situation. The IAD with noisy data needs more research in the future.

**Continual IAD.** Work integrating continual learning (CL)

is growing with the development of anomaly detection. The first CL benchmark for industrial IAD is introduced by Li *et al.* [45], but their setting ignores the large domain gap of different datasets. To further explore the ability of IAD methods, more efforts should be made in this setting.

### III. IM-IAD

In this section, we first present the definition of five settings in IM-IAD, and then summarize the implementation details of baseline methods, mainstream datasets, evaluation metrics, and hyperparameters. Finally, we point out the importance of studying IM-IAD from a uniform perspective.

#### A. Problem Definition

The goal of IAD is that, given a normal or abnormal sample from a target category, the anomaly detection model should predict whether or not the image is anomalous and localize the anomaly region if the prediction result is anomalous. We provide the following five settings.

- 1) **Unsupervised IAD.** The training set consists only of  $m$  normal samples for each category. The test set contains normal and abnormal samples.
- 2) **Fully supervised IAD.** The training set consists of  $m$  normal samples and  $n$  abnormal samples, where  $n \ll m$ . In our case, we set  $n$  as 10.
- 3) **Few-shot IAD.** Given a training set of only  $m$  normal samples, where  $m \leq 8$ , from a certain category. The

TABLE II  
REPRESENTATIVE ALGORITHMS FOR IM-IAD. THE PURPLE ONES INDICATE OUR RE-IMPLEMENTATION METHODS.

Paradigm			Methods
Vanilla	Feature embedding	Normalizing flow	CS-Flow [62], FastFlow [86], CFlow [27], DifferNet [61]
		Memory bank	PaDiM [20], PatchCore [60], SPADE [15], CFA [40], SOMAD [44], [37]
		Teacher-student	RD4AD [23], STPM [74], [78], [5], [63]
		One-class classification	CutPaste [42], PANDA [58], DROC[68], MOCCA [51],PatchSVDD [83], SE-SVDD [30], [64]
	Reconstruction	External data usage	DREAM [88], DSR [90], MSTUnet[34], DFR [81]
		Internal data usage only	FAVAE [21], NSA [65], RIAD [89], SCADN [79], InTra [55], [7], [29], [48], [16], [80], [22]
Fully supervised			DRA [25], DevNet [54], PRN [91], BGAD [82], SemiRESt [43], FCDD [50], SPD [94], CAVGA [73], [14]
Few-shot			RegAD [31], RFS [36], [67]
Noisy label			IGD [11], LOE [56], TrustMAE [70], SROC [17], SRR [85], CPCAD [19]
Continual			DNE [45]

number of  $m$  could be 1, 2, 4, and 8 for the target category, respectively.

- 4) **Noisy IAD.** Given a training set of  $m$  normal samples and  $n$  abnormal samples,  $n$  most of 20% of  $m + n$ . And  $n$  abnormal samples are labeled as normal samples for the training dataset.
- 5) **Continual IAD.** Given a finite sequence of training dataset  $\mathcal{T}_{train}^{total}$  consists of  $n$  categories,  $\mathcal{T}_{train}^{total} = \{\mathcal{T}_{train}^1, \mathcal{T}_{train}^2, \dots, \mathcal{T}_{train}^n\}$ , i.e.,  $\mathcal{T}_{train}^{total} = \bigcup_{i=1}^n \mathcal{T}_{train}^i$ , where the subsets  $\mathcal{T}_{train}^i$  consists of normal samples from one certain category  $c_i, i \in n$ . The IAD algorithm is trained once for each category dataset  $\mathcal{T}_{train}^i$  in the CL scenario. During the test, the updated model is evaluated on each category of previous datasets  $\mathcal{T}_{test}^{total}$ , i.e.,  $\mathcal{T}_{test}^{total} = \{\mathcal{T}_{test}^1, \mathcal{T}_{test}^2, \dots, \mathcal{T}_{test}^{i-1}\}$ , respectively.

### B. Implementation Details

1) **Baseline Methods:** Table II lists 16 IAD algorithms (marked in purple). The criteria for selecting algorithms to be implemented for IM-IAD are that the algorithms should be representative in terms of supervision level (fully supervised and unsupervised), noise-resilient capabilities, the facility of data-efficient adaptation (few shot), and the capacity to overcome catastrophic forgetting. Since most of them achieve state-of-the-art (SOTA) performance on the majority of industrial image datasets, they are referred to as vanilla methods and compared in the IM setting.

2) **Datasets:** To perform comprehensive ablation studies, we employ 7 public datasets in the IM setting, including MVTEC AD [4], [2], MVTEC LOCO-AD [3] MPDD [33], BTAD [52], VisA [94], MTD [32], and DAGM [18]. Table III provides an overview of these datasets, including the number of samples (normal and abnormal samples), the number of classes, the types of anomalies, and the resolution of the image. Pixel-level annotations are available for all datasets. Note that DAGM is a synthetic dataset, MVTEC LOCO-AD proposes logical IAD, and VisA proposes multi-instance IAD.

3) **Evaluation Metrics:** In terms of structural anomalies, we employ Area Under the Receiver Operating Characteristics (AU-ROC/AUC), Area Under Precision-Recall (AUPR/AP), and PRO [2] to evaluate the abilities of anomaly localization. Regarding logical anomalies, we adopt sPRO [6] to measure the ability of logical defect detection. Additionally, we use the

TABLE III  
COMPARISON OF DATASETS IN IM-IAD.

Dataset	Sample Number		Classes		Image Resolution	
	Normal	Anomaly	Anomaly Type	Object	Min	Max
MVTec AD [4], [2]	4,096	1,258	73	15	700	1,024
MVTec LOCO-AD [3]	2,651	993	89	5	850	1,700
MPDD [33]	1,064	282	5	1	1,024	1,024
BTAD [52]	2,250	580	3	3	600	1,600
MTD [32]	952	392	5	1	113	491
VisA [94]	10,621	1,200	78	12	960	1,562
DAGM [18]	15,000	2,100	10	10	512	512

Forgetting Measure (FM) [10] to assess the ability to resist catastrophic forgetting. The relevant formulas are shown in Table IV.

4) **Hyperparameters:** Table V shows the hyperparameter settings of IM-IAD, including training epochs, batch size, image size, and learning rate, respectively. We share the source codes on the website: <https://github.com/M-3LAB/open-iad>.

### C. Uniform Perspective

The proposed IM-IAD bridges the connection of different existing settings, as there is no uniform evaluation benchmark.

1) From the perspective of training datasets, the type and number of instances are the main differences between the five settings shown in Fig. 1. It should be noted that unsupervised IAD is based on normal samples for training purposes. On the contrary, both fully supervised IAD and noisy IAD incorporate a limited quantity of abnormal samples during the training phase. Few-shot IAD employs a limited number of normal samples ( $\leq 8$ ) for training.

2) From the perspective of applications, these settings are designed to accommodate different scenarios in the real world. Unsupervised IAD focuses on detecting anomalies in a general scenario, and collecting large amounts of abnormal samples for training purposes is difficult. The few-shot IAD aims to solve the challenge of cold start in a single assembly line scenario, where normal samples are limited. The goal of continual IAD is to address catastrophic forgetting that occurs when IAD models are integrated into the recycling assembly line. Noisy IAD tries to eliminate the side effects resulting from contaminated training data. Full supervision is aimed at improving the efficiency of abnormal sample utilization because labelling anomalies is expensive.

TABLE IV  
A SUMMARY OF METRICS USED IN IM-IAD.

Metric	Better	Formula	Remarks / Usage
Precision (P)	↑	$P = TP / (TP + FP)$	True Positive (TP), False Positive (FP)
Recall (R)	↑	$R = TP / (TP + FN)$	False Negative (FN)
True Positive Rate (TPR)	↑	$TPR = TP / (TP + FN)$	Classification
False Positive Rate (FPR)	↓	$FPR = FP / (FP + TN)$	True Negative (TN)
Area Under the Receiver Operating Characteristic curve (AU-ROC) [2]	↑	$\int_0^1 (TPR) d(FPR)$	Classification
Area Under Precision-Recall (AU-PR) [2]	↑	$\int_0^1 (P) d(R)$	Localization, Segmentation
Per-Region Overlap (PRO) [2]	↑	$PRO = \frac{1}{N} \sum_i \sum_k \frac{P_i \cap C_{i,k}}{C_{i,k}}$	Total ground-truth number (N), Predicted abnormal pixels (P), Defect ground-truth regions (C), Segmentation
Saturated Per-Region Overlap (sPRO) [6]	↑	$sPRO(P) = \frac{1}{m} \sum_{i=1}^m \min(\frac{A_i \cap P}{s_i}, 1)$	Total ground-truth number (m), Predicted abnormal pixels (P), Defect ground-truth regions (A), Corresponding saturation thresholds (s), Segmentation
Forgetting Measure (FM) [10]	↓	$FM_j^k = \max_{l \in \{1, \dots, k-1\}} T_{l,j} - T_{k,j}$	Task (T), Number of tasks (k), Task to be evaluated (j)

TABLE V  
DETAILS OF EXPERIMENTAL SETTINGS.

Method	CFA	CSFlow	CutPaste	DNE	DRAEM	FastFlow	FAVAE	IGD	PaDiM	PatchCore	RegAD	RD4AD	SPADE	STPM
Training Epochs	50	240	256	50	700	500	100	256	1	1	50	200	1	100
Batch Size	4	16	32	32	8	32	64	16	32	2	32	8	8	8
Image Size	256	768	224	224	256	256	256	256	256	256	224	256	256	256
Learning Rate	0.001	0.0002	0.0001	0.0001	0.0001	0.001	0.00001	0.0001	\	\	0.0001	0.005	\	0.4

### D. Open Challenges

Regarding our IM-IAD setting, the following is a summary of the challenging issues that need to be investigated.

1) The remaining challenges for fully supervised IAD [25], [43] described in Fig. 1(c) is how to effectively use the guidance of limited abnormal data and a large number of normal samples to detect the anomalies.

2) For the few-shot IAD shown in Fig. 1(d), we aim to detect anomalies in the test set using a small number of normal or abnormal images in the training set [77]. The main obstacles are i) In a few-shot setting, the training dataset for each category contains only normal samples, which means that there are no annotations at the image or pixel level. ii) Few normal samples of the training set are accessible. In the setting we propose, there are less than eight training samples.

3) We attempt to detect abnormal samples and identify anomalies given a target category for IAD in the presence of noise [35] described in Fig. 1(e). For example, it is assumed that clean training data consists exclusively of normal samples. While contaminated training data contains noisy samples that are incorrectly labeled as normal, *i.e.*, label flipping. Anormal samples are easily mislabeled as normal because the anomalies are too small to identify. The most significant barriers are summarized as follows. i) Each category's training set contains noisy data that could easily confuse the decision threshold of IAD algorithms. ii) There is a large amount of noisy data. Here, the percentage of anomalous samples in the training set ranges from 5% to 20%. Hence, the objective of noisy IAD is to assess the resilience of current unsupervised IAD methods in the presence of contaminated data.

4) For the continual IAD presented in Fig. 1(f), the greatest challenge is that IAD algorithms may suffer from catastrophic forgetting when they have completed training on the new category dataset. In real-world applications, a single assembly line

typically accommodates a substantial amount of workpiece, often containing thousands. The deployment of numerous IAD models on a single assembly line is unfeasible due to high expenses associated with maintenance. Furthermore, a large part of the assembly line process involves recycling. Hence, industrial deployment requires IAD models to overcome catastrophic forgetting.

## IV. RESULTS AND DISCUSSIONS

This section explores existing algorithms and discusses the important aspects of the proposed uniform settings. Each part describes experimental facilities, analyzes results, and provides other challenges and future directions.

### A. Overall Comparisons

**Settings.** The vanilla methods are presented in Table II. The unsupervised setting is described in Sec. III-A-1.

**Discussions.** The statistical results of Table VI indicate that there is no single winner for all datasets. Furthermore, Fig. 2(a) and Fig. 2(b) show that there are no dominant solutions to GPU accuracy, inference speed, and memory. Specifically, Table VI indicates that PatchCore, one of the most advanced memory bank based methods, performs better on MVTec AD than on MVTec LOCO-AD. Because PatchCore architectures specialize in structural anomalies, not logical anomalies, the main differences between MVTec AD and MVTec LOCO-AD are the types of anomalies.

**Logical Anomaly Definition.** MVTec LOCO-AD consists of structural and logical anomalies. Logical anomalies are not dents or scratches, but are caused by displacement or missing parts. However, MVTec AD only has a structural abnormality. For visualization results, Fig. 3 shows the restrictions of each IAD model to different types of anomalies. For example, the



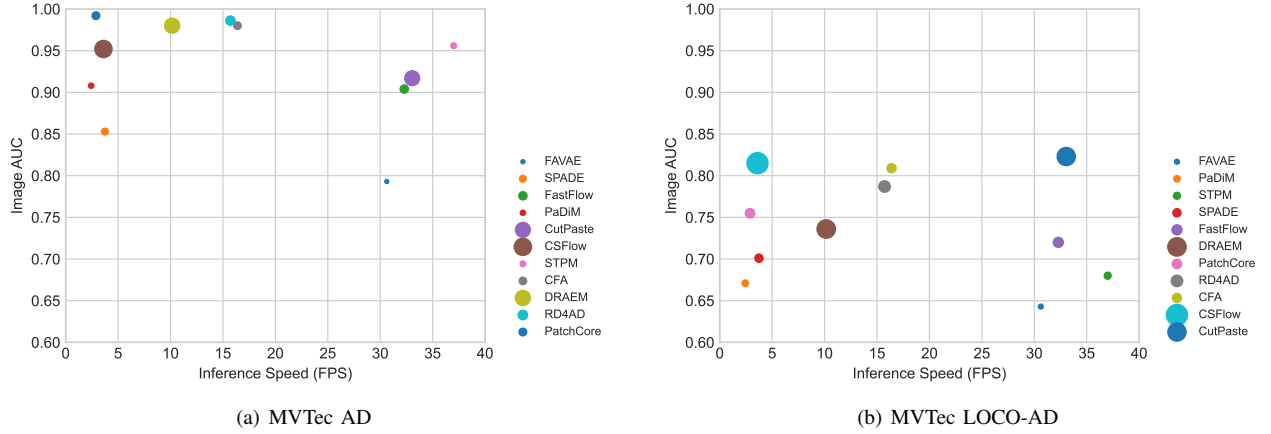


Fig. 2. Visualization of vanilla IAD algorithms on Image AUC  $\uparrow$ , inference time and GPU memory under MVTEC AD and LOCO-AD. The Y-axis denotes the performance of the IAD model. The X-axis refers to the inference time taken for each image. The size of the circle denotes the GPU memory consumption of the IAD model during the test phase, where the small one is better.

fifth-column images are screw bags, and their defects are logical anomalies. In particular, each box of non-defective screw bags contains exactly *one pushpin*. However, the defective screw bag contains two pushpins in the upper right corner of the box. The patchcore heatmap cannot accurately represent the anomaly on the right, *i.e.*, whereas RD4AD [23] can precisely identify the logical anomaly on the top right.

**Memory Usage and Inference Speed.** From Fig. 2, it is clear that there are no dominant IAD methods in terms of accuracy, memory usage and inference time. PatchCore achieves SOTA performance in image AUC, but does not take advantage of memory usage and inference time. In practical scenarios, the use of memory and the speed of inference must be fully taken into account. Therefore, current advanced IAD algorithms cannot meet the requirements of IM.

**Image-Level or Pixel-Level Evaluation?** Both image-level and pixel-level metrics are commonly used by researchers to evaluate the classification performance of IAD algorithms. In practice, the image-level metric is used to judge whether the whole product is abnormal or not, while the pixel-level metric is used to indicate anomaly localization performance. To be specific, the pixel-level metric can evaluate the degree of defect, which is strongly associated with the price of products. A lower degree of defects implies a higher price, or vice versa. According to Table VI, we discover that certain IAD methods, like PatchCore, perform well on image AUROC but poorly on pixel AP, or vice versa. These two types of metrics signify distinct capabilities of IAD algorithms, and both are very important for IM. Therefore, to comprehensively evaluate the model's performance, we hope to see future models that excel in both image-level and pixel-level performance.

**Challenges.** How to use the types of visual anomalies to select and design unsupervised algorithms effectively? Algorithm selection based on anomalous types is crucial, but there is a lack of research in this area. Due to the low failure rate of production lines, it is difficult to collect a large number of abnormal samples for the supervision of training in IM. However, since product line specialists can provide information on the type of anomalies, it is appropriate to be aware of the type

of visual anomalies in advance. In other words, knowledge of anomalous types in an unsupervised algorithm can be considered as supervision information. Therefore, algorithm designers should consider anomalous types when developing algorithms.

#### B. Role of Global Features in Logical IAD

**Settings.** We benchmark the vanilla unsupervised IAD algorithms on the MVTEC LOCO-AD dataset. In addition, we have re-implemented the baseline logical AD method, GCAD [3].

**Discussions.** According to Table VII, we find that the baseline method GCAD [3] is superior to all unsupervised IAD methods. The key idea of GCAD [3] is to encode each pixel's feature descriptor through a bottleneck architecture into a global feature. Existing unsupervised IAD approaches have the disadvantage that their architectures are not optimized to acquire global features.

**Challenges.** To achieve a high detection performance for logical IAD tasks, global feature extraction is crucial. The statistical results presented in Table VII highlight the significance of global anomaly feature extraction. Recent network architectures such as Transformer [26] and Normalizing Flow [39] focus on long-distance feature extraction, which makes it easier to detect logical anomalies. The results in Table VII show that CSFlow [62], which is based on Normalizing Flow, achieves the second-best performance in terms of logical anomalies, indicating its potential. Additionally, the bottleneck architecture is another feasible approach to capturing global features. As demonstrated by the heat map on the logical anomaly dataset in Fig. 3, the bottleneck design of RD4AD [23] is capable of extracting global features.

#### C. Abnormal Data for Fully Supervised IAD

**Settings.** We first benchmark fully supervised IAD methods according to the setting in [54], [12], [43]. According to the definition of fully supervised IAD in Sec. III-A-2, we have set the number of abnormal training samples to 10. Here, we

TABLE VI

COMPARISON OF VANILLA IAD ALGORITHMS FOR 7 DATASETS USING 5 METRICS. WE REPORT SPRO WITH A 0.05 INTEGRATION PARAMETER. THE BEST AND SECOND-BEST RESULTS ARE MARKED IN RED AND BLUE, RESPECTIVELY.

Dataset	Metric $\uparrow$	CFA	CS-Flow	CutPaste	DRAEM	FastFlow	FAVAE	PaDiM	PatchCore	RD4AD	SPADE	STPM
MVTec AD	Image AUC	0.981	0.952	0.918	0.981	0.905	0.793	0.908	<b>0.992</b>	<b>0.986</b>	0.854	0.924
	Image AP	0.993	0.975	0.965	0.990	0.945	0.913	0.954	<b>0.998</b>	<b>0.995</b>	0.940	0.957
	Pixel AUC	0.971	–	–	<b>0.975</b>	0.955	0.889	0.966	0.994	<b>0.978</b>	0.955	0.954
	Pixel AP	0.538	–	–	<b>0.689</b>	0.398	0.307	0.452	0.561	<b>0.580</b>	0.471	0.518
	Pixel PRO	0.898	–	–	0.921	0.856	0.749	0.913	<b>0.943</b>	<b>0.939</b>	0.895	0.879
MVTec LOCO-AD	Image AUC	0.814	0.814	0.734	0.798	0.639	0.623	0.780	<b>0.835</b>	<b>0.867</b>	0.687	0.679
	Image AP	0.944	0.942	0.915	0.933	0.866	0.873	0.927	<b>0.948</b>	<b>0.958</b>	0.890	0.891
	Pixel AUC	0.908	–	–	0.942	0.796	0.944	<b>0.987</b>	<b>0.990</b>	0.971	0.971	0.848
	Pixel AP	0.219	–	–	0.209	0.053	0.099	0.149	0.150	<b>0.342</b>	<b>0.261</b>	0.164
	Mean sPRO	<b>0.581</b>	–	–	0.426	0.357	0.446	0.521	0.343	<b>0.637</b>	0.520	0.428
MPDD	Image AUC	0.923	<b>0.973</b>	0.771	0.941	0.887	0.570	0.706	<b>0.948</b>	0.927	0.784	0.876
	Image AP	0.922	<b>0.968</b>	0.800	0.961	0.881	0.705	0.784	<b>0.970</b>	0.953	0.815	0.914
	Pixel AUC	0.948	–	–	0.918	0.808	0.906	0.955	<b>0.990</b>	<b>0.987</b>	0.982	0.981
	Pixel AP	0.283	–	–	0.288	0.115	0.088	0.155	<b>0.432</b>	<b>0.455</b>	0.342	0.354
	Pixel PRO	0.832	–	–	0.781	0.498	0.706	0.848	<b>0.939</b>	<b>0.953</b>	0.926	<b>0.939</b>
BTAD	Image AUC	0.938	0.936	0.917	0.895	0.919	0.923	<b>0.965</b>	<b>0.947</b>	0.937	0.904	0.918
	Image AP	0.980	0.890	0.953	0.974	0.867	<b>0.986</b>	0.976	<b>0.989</b>	0.985	0.974	0.962
	Pixel AUC	0.959	–	–	0.874	0.965	0.949	<b>0.977</b>	<b>0.978</b>	0.958	0.950	0.937
	Pixel AP	0.517	–	–	0.159	0.379	0.349	<b>0.535</b>	<b>0.520</b>	0.517	0.441	0.401
	Pixel PRO	0.702	–	–	0.629	0.725	0.713	<b>0.798</b>	<b>0.752</b>	0.723	0.745	0.667
MTD	Image AUC	<b>0.913</b>	0.887	0.830	0.782	0.891	0.795	0.885	<b>0.975</b>	0.884	0.868	0.729
	Image AP	<b>0.959</b>	0.945	0.912	0.885	0.947	0.867	0.944	<b>0.988</b>	0.947	0.928	0.847
	Pixel AUC	0.731	–	–	0.660	0.710	0.735	<b>0.768</b>	<b>0.836</b>	0.693	0.742	0.642
	Pixel AP	0.246	–	–	0.148	0.172	0.120	<b>0.768</b>	<b>0.303</b>	0.218	0.123	0.102
	Pixel PRO	0.528	–	–	0.541	0.568	0.632	<b>0.798</b>	<b>0.686</b>	0.623	0.627	0.478
VisA	Image AUC	0.920	0.744	0.819	0.887	0.822	0.803	0.891	<b>0.951</b>	<b>0.960</b>	0.821	0.833
	Image AP	0.935	0.787	0.848	0.905	0.843	0.843	0.895	<b>0.962</b>	<b>0.965</b>	0.847	0.873
	Pixel AUC	0.843	–	–	0.935	0.882	0.880	<b>0.981</b>	<b>0.988</b>	0.901	0.856	0.834
	Pixel AP	0.268	–	–	0.265	0.156	0.213	<b>0.309</b>	<b>0.401</b>	0.277	0.215	0.169
	Pixel PRO	0.551	–	–	0.724	0.598	0.679	<b>0.859</b>	<b>0.912</b>	0.709	0.659	0.620
DAGM	Image AUC	<b>0.948</b>	0.752	0.839	0.908	0.874	0.695	0.940	0.936	<b>0.958</b>	0.714	0.739
	Image AP	<b>0.878</b>	0.781	0.680	0.790	0.699	0.376	0.811	0.826	<b>0.901</b>	0.392	0.498
	Pixel AUC	0.942	–	–	0.868	0.911	0.804	0.961	<b>0.967</b>	<b>0.975</b>	0.880	0.859
	Pixel AP	0.495	–	–	0.306	0.342	0.170	0.492	<b>0.517</b>	<b>0.534</b>	0.133	0.151
	Pixel PRO	0.870	–	–	0.710	0.799	0.600	<b>0.906</b>	0.893	<b>0.930</b>	0.707	0.668

TABLE VII

BENCHMARK ON MVTec LOCO-AD IN TERMS OF LOGICAL ANOMALIES, STRUCTURAL ANOMALIES AND THEIR MEAN VALUE. THE BEST AND SECOND-BEST RESULTS ARE MARKED IN RED AND BLUE, RESPECTIVELY.

Method	Image AUROC $\uparrow$			Pixel sPRO $\uparrow$		
	Logical	Structural	Mean	Logical	Structural	Mean
PatchCore	0.690	0.820	0.755	0.340	0.345	0.343
CFA	0.768	0.851	0.809	<b>0.536</b>	0.625	0.581
SPADE	0.653	0.749	0.701	0.430	0.609	0.520
PaDiM	0.637	0.705	0.671	0.517	0.525	0.521
RD4AD	0.694	<b>0.880</b>	0.787	0.497	<b>0.777</b>	<b>0.637</b>
STPM	0.597	0.763	0.680	0.328	0.529	0.428
CutPaste	0.779	<b>0.867</b>	<b>0.823</b>	–	–	–
CSFlow	<b>0.783</b>	0.847	0.815	–	–	–
FastFlow	0.727	0.712	0.720	0.359	0.356	0.357
DRAEM	0.728	0.744	0.736	0.454	0.398	0.426
FAVAE	0.659	0.628	0.643	0.501	0.392	0.446
GCAD	<b>0.860</b>	0.806	<b>0.833</b>	<b>0.711</b>	<b>0.692</b>	<b>0.701</b>

make comparisons with PRN [91], BGAD [82], DevNet [54], DRA [25], SemiREST [43], and PatchCore [60].

**Discussions.** Fully supervised IAD algorithms use the distance between test and training samples to predict anomalies. The core idea is that the features of abnormal and normal

samples are very different. For example, DevNet [54] proposes using the deviation loss function to enforce the statistical deviation of all anomalies from normal samples. From Table VIII, we can see that the performance of fully supervised IAD methods exceeds that of unsupervised methods (such as PatchCore) in pixel levels by a large margin. It justifies the effectiveness of incorporating an abnormal sample for training.

**Challenges.** It is essential to improve the efficacy of the abnormal samples for the fully supervised IAD method. Because of the high cost associated with anomaly labels in real applications. On average, each worker spends three hours completing the pixel labels for each image. In subsequent research, researchers have to develop an improved fully supervised IAD algorithm with greater efficiency. The algorithm should reduce the number of abnormal samples for training while maintaining IAD accuracy.

#### D. Rotation Augmentation for Feature-Embedding based Few-Shot IAD

**Settings.** With respect to the training samples, we choose 1, 2, 4, and 8 to benchmark vanilla IAD methods. Details can be found in the few-shot setting of Sec. III-A-3. In addition, we

TABLE VIII  
PERFORMANCE ON THE FULLY-SUPERVISED SETTING. THE BEST AND SECOND-BEST RESULTS ARE MARKED IN RED AND BLUE, RESPECTIVELY.

Method	Metric $\uparrow$	Bottle	Cable	Capsule	Carpet	Grid	Hazelnut	Leather	Metal_nut	Pill	Screw	Tile	Toothbrush	Transistor	Wood	Zipper	Mean
PRN	Pixel AUC	<b>0.994</b>	<b>0.988</b>	0.985	0.990	0.984	<b>0.997</b>	0.997	<b>0.997</b>	<b>0.995</b>	0.975	<b>0.996</b>	<b>0.996</b>	<b>0.984</b>	0.978	0.988	0.990
	Pixel AP	<b>0.923</b>	0.789	<b>0.622</b>	0.820	0.457	<b>0.938</b>	0.697	<b>0.980</b>	<b>0.913</b>	0.449	<b>0.965</b>	<b>0.781</b>	<b>0.856</b>	<b>0.826</b>	0.776	<b>0.786</b>
	Pixel PRO	0.970	<b>0.972</b>	0.925	<b>0.970</b>	0.959	0.974	<b>0.992</b>	0.958	<b>0.972</b>	0.924	<b>0.982</b>	0.956	0.948	0.959	0.955	0.961
BGAD	Pixel AUC	0.993	0.985	<b>0.988</b>	<b>0.996</b>	0.984	0.994	<b>0.998</b>	0.996	0.995	<b>0.993</b>	0.993	<b>0.995</b>	0.979	<b>0.980</b>	<b>0.993</b>	0.992
	Pixel AP	0.871	0.814	0.583	<b>0.832</b>	<b>0.592</b>	0.824	<b>0.755</b>	0.973	<b>0.921</b>	<b>0.553</b>	0.940	0.713	0.823	0.787	<b>0.782</b>	0.784
	Pixel PRO	<b>0.971</b>	<b>0.977</b>	<b>0.968</b>	0.989	<b>0.987</b>	<b>0.986</b>	0.995	<b>0.968</b>	0.987	<b>0.968</b>	0.979	<b>0.964</b>	<b>0.971</b>	<b>0.968</b>	<b>0.977</b>	<b>0.977</b>
DevNet	Pixel AUC	0.939	<b>0.888</b>	0.918	0.972	0.879	0.911	0.942	0.778	0.826	0.603	0.927	0.846	0.560	0.864	0.937	0.853
	Pixel AP	0.515	0.360	0.155	0.457	0.255	0.221	0.081	0.356	0.146	0.014	0.523	0.067	0.064	0.251	0.196	0.244
	Pixel PRO	0.835	0.809	0.836	0.858	0.798	0.836	0.885	0.769	0.692	0.311	0.789	0.335	0.391	0.754	0.813	0.714
DRA	Pixel AUC	0.913	0.866	0.893	0.982	0.860	0.896	0.938	0.795	0.845	0.540	0.923	0.755	0.791	0.829	0.969	0.853
	Pixel AP	0.412	0.347	0.117	0.523	0.268	0.225	0.056	0.299	0.216	0.050	0.576	0.045	0.110	0.227	0.429	0.260
	Pixel PRO	0.776	0.777	0.791	0.922	0.715	0.869	0.840	0.767	0.770	0.301	0.815	0.561	0.490	0.697	0.910	0.733
SemiREST	Pixel AUC	<b>0.995</b>	<b>0.992</b>	<b>0.988</b>	<b>0.997</b>	<b>0.994</b>	<b>0.998</b>	<b>0.999</b>	<b>0.999</b>	<b>0.993</b>	<b>0.998</b>	<b>0.997</b>	<b>0.996</b>	<b>0.986</b>	<b>0.992</b>	<b>0.997</b>	<b>0.995</b>
	Pixel AP	<b>0.936</b>	<b>0.895</b>	<b>0.600</b>	<b>0.891</b>	<b>0.664</b>	<b>0.922</b>	<b>0.817</b>	<b>0.991</b>	<b>0.861</b>	<b>0.721</b>	<b>0.969</b>	<b>0.742</b>	<b>0.855</b>	<b>0.887</b>	<b>0.910</b>	<b>0.844</b>
	Pixel PRO	<b>0.985</b>	0.959	0.970	<b>0.991</b>	<b>0.970</b>	<b>0.983</b>	<b>0.997</b>	<b>0.982</b>	<b>0.989</b>	<b>0.988</b>	<b>0.989</b>	<b>0.971</b>	<b>0.978</b>	<b>0.979</b>	<b>0.992</b>	<b>0.981</b>
PatchCore	Pixel AUC	0.988	0.988	<b>0.992</b>	0.992	<b>0.990</b>	0.990	0.994	0.987	0.983	0.996	0.964	0.988	0.961	0.949	0.990	<b>0.994</b>
	Pixel AP	0.768	0.653	0.442	0.627	0.325	0.537	0.456	0.870	0.777	0.354	0.546	0.372	0.610	0.477	0.595	0.561
	Pixel PRO	0.957	0.945	<b>0.958</b>	0.949	0.939	0.958	0.974	0.954	0.945	0.964	0.906	0.918	0.906	0.914	0.961	0.943

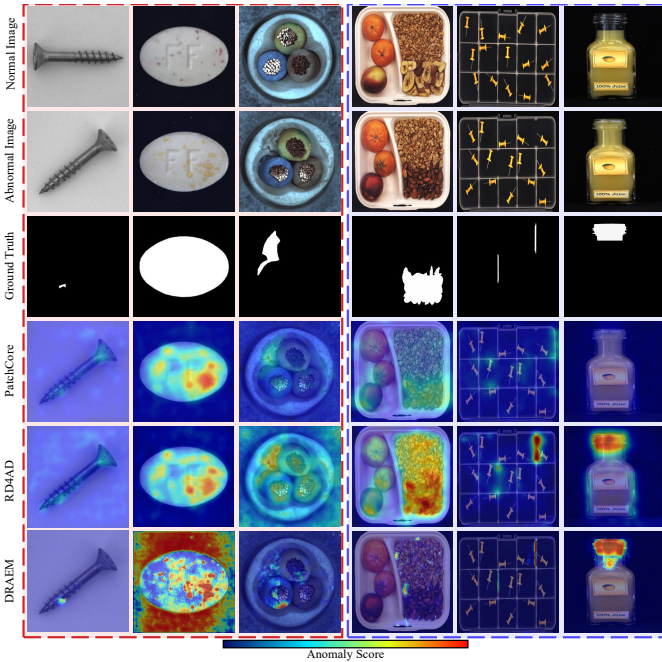


Fig. 3. Visualization of the representative vanilla IAD algorithms. The three columns on the left (marked in red) show structural anomalies, while the three columns on the right (marked in blue) show logical anomalies. The first row indicates the training images, where all training images are normal. The second row denotes a test abnormal image and the third row reveals the anomalies of the above abnormal image. Lastly, the fourth to sixth row presents the heat map of PatchCore, RD4AD and DRAEM, respectively.

make a comparison with RegAD [31], which is an advanced method of meta-learning.

**Discussions.** Fig. 4 shows that CutPaste, STPM, and PatchCore’s performance is comparable to the base model RegAD. Inspired by [53] and [13], we try to improve performance in IM few-shot settings using data augmentation. The statistical results of Table IX indicate that most data augmentation methods are sufficient to improve the few-shot IAD performance. Further, we find that rotation is an optimal augmentation method because most of the real-time industrial image [4], [33] could be transformed into another image by rotation, such as metal\_nut and screw.

TABLE IX  
IMAGE-LEVEL AUC-ROC  $\uparrow$  ON MVTEC AD. THE BEST AND SECOND-BEST RESULTS ARE MARKED IN RED AND BLUE, RESPECTIVELY.

Shot	Method	Vanilla	Rotation	Flip	Scale	Translate	ColorJitter	Perspective
1	CFA	0.811	<b>0.829</b>	0.811	0.788	0.802	<b>0.814</b>	0.806
	CSFlow	0.708	0.727	0.708	<b>0.742</b>	<b>0.750</b>	0.700	0.713
	CutPaste	0.650	0.701	<b>0.702</b>	0.680	0.679	0.652	<b>0.703</b>
	DRAEM	0.683	<b>0.718</b>	0.715	0.714	0.690	0.687	<b>0.741</b>
	FastFlow	0.527	0.618	0.613	<b>0.694</b>	<b>0.682</b>	0.578	0.600
	FAVAE	0.651	0.560	<b>0.591</b>	0.600	0.581	0.588	<b>0.626</b>
	PaDiM	<b>0.684</b>	<b>0.697</b>	0.683	0.669	0.683	0.681	0.674
	PatchCore	0.788	<b>0.805</b>	0.792	0.788	<b>0.800</b>	0.797	0.789
	RD4AD	0.770	0.805	0.802	0.799	<b>0.823</b>	<b>0.816</b>	0.784
	SPADE	—	—	—	—	—	—	—
	STPM	0.799	<b>0.841</b>	0.814	0.823	<b>0.843</b>	0.831	0.840
2	CFA	0.839	<b>0.860</b>	<b>0.853</b>	0.795	0.825	0.833	0.843
	CSFlow	0.745	<b>0.781</b>	0.773	<b>0.783</b>	0.768	0.754	0.778
	CutPaste	0.697	0.709	<b>0.748</b>	0.659	0.659	0.611	<b>0.726</b>
	DRAEM	0.780	0.765	<b>0.774</b>	0.751	0.771	0.773	<b>0.784</b>
	FastFlow	0.555	<b>0.743</b>	0.674	<b>0.753</b>	0.731	0.628	0.617
	FAVAE	0.667	<b>0.648</b>	<b>0.659</b>	0.595	0.620	0.642	0.631
	PaDiM	0.708	<b>0.734</b>	<b>0.731</b>	0.694	0.716	0.710	0.714
	PatchCore	0.795	<b>0.831</b>	0.805	0.796	<b>0.806</b>	0.793	0.802
	RD4AD	0.798	<b>0.832</b>	0.816	<b>0.835</b>	0.817	<b>0.835</b>	0.820
	SPADE	—	0.737	0.731	0.710	0.734	0.733	0.744
	STPM	0.840	0.839	<b>0.850</b>	0.848	<b>0.851</b>	0.849	0.838
4	CFA	0.879	<b>0.891</b>	0.861	0.818	0.860	<b>0.895</b>	0.883
	CSFlow	0.785	<b>0.841</b>	0.815	<b>0.825</b>	0.810	0.806	0.738
	CutPaste	0.728	<b>0.771</b>	<b>0.714</b>	0.519	0.674	0.621	0.671
	DRAEM	0.820	0.798	0.802	0.819	<b>0.824</b>	0.823	<b>0.826</b>
	FastFlow	0.693	0.741	0.745	<b>0.790</b>	<b>0.782</b>	0.723	0.734
	FAVAE	0.655	0.626	<b>0.669</b>	0.605	0.639	<b>0.670</b>	<b>0.623</b>
	PaDiM	0.722	<b>0.734</b>	0.723	0.689	0.720	<b>0.727</b>	0.716
	PatchCore	0.844	<b>0.872</b>	0.826	0.844	0.848	<b>0.852</b>	0.847
	RD4AD	0.838	<b>0.897</b>	0.871	0.866	<b>0.876</b>	0.872	0.861
	SPADE	—	<b>0.764</b>	0.739	0.749	0.758	0.757	<b>0.759</b>
	STPM	0.864	0.869	0.865	<b>0.876</b>	0.875	0.868	<b>0.885</b>
8	CFA	0.923	0.913	0.888	0.875	<b>0.920</b>	0.919	<b>0.924</b>
	CSFlow	0.856	<b>0.900</b>	0.863	<b>0.900</b>	<b>0.893</b>	0.892	0.861
	CutPaste	0.705	<b>0.808</b>	<b>0.857</b>	0.473	0.694	0.607	0.673
	DRAEM	0.872	0.892	<b>0.905</b>	0.892	0.900	0.904	<b>0.919</b>
	FastFlow	0.828	0.809	0.793	<b>0.843</b>	<b>0.826</b>	0.809	0.810
	FAVAE	0.701	0.651	<b>0.670</b>	0.619	0.611	<b>0.680</b>	0.668
	PaDiM	0.776	<b>0.810</b>	0.739	0.734	0.761	<b>0.779</b>	0.771
	PatchCore	0.891	<b>0.916</b>	0.876	0.889	0.898	0.883	<b>0.891</b>
	RD4AD	0.903	<b>0.933</b>	0.911	0.917	<b>0.921</b>	0.912	0.916
	SPADE	0.781	<b>0.794</b>	0.770	0.783	<b>0.791</b>	0.788	0.787
	STPM	0.865	0.896	0.870	0.910	<b>0.914</b>	<b>0.912</b>	0.904



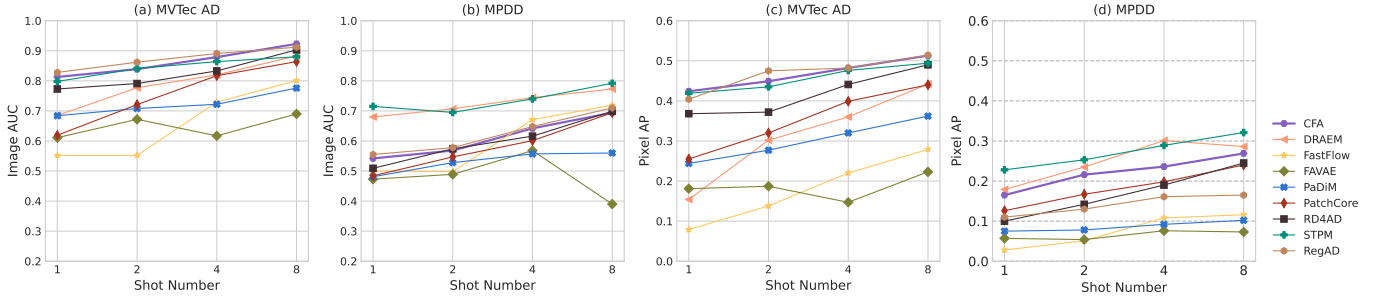


Fig. 4. Few-shot IAD Benchmark on MVTEC AD and MPDD. The Y-axis refers to the metric value and the X-axis denotes the shot number.

**Challenges.** Synthesis of abnormal samples is important but difficult. Previously, researchers focused on developing data augmentation methods for normal images. However, little effort is made to synthesize abnormal samples. Because of the fault-free production line in industrial environments, it is very difficult to collect large quantities of abnormal samples. In the future, more attention should be paid to abnormal synthesizing methods, such as CutPaste [42] and DRAEM [88].

#### E. Importance Re-weighting for Noisy IAD

**Settings.** Using the noise setting introduced in Sec. III-A-4, we create a noisy label training dataset by injecting a variety of abnormal samples from the original test set. Specifically, we borrowed the settings from SoftPatch [35]. The abnormal sample accounts for mainly 20% of all training data (called noise ratio). The noise ratio is 5% to 20% and its step size is 5%. Due to the limited size of the test category, we selected a training sample of up to 75% of the abnormal sample of the test dataset. At the training stage, the labels observed in all training datasets are normal. During the test phase, abnormal samples are no longer evaluated. In the noise settings, we benchmark the vanilla and noisy IAD baseline method, IGD [11].

TABLE X

IMAGE AUC  $\uparrow$  OF NOISY IAD METHODS ON MVTEC AD AND MPDD UNDER VARIOUS NOISE RATIOS. THE BEST AND SECOND-BEST RESULTS ARE MARKED IN RED AND BLUE, RESPECTIVELY.

Dataset	MVTEC AD				MPDD			
	0.05	0.1	0.15	0.2	0.05	0.1	0.15	0.2
CFA	0.969	0.962	0.949	0.946	0.894	0.808	0.839	0.782
CS-Flow	0.939	0.894	0.904	0.874	0.773	0.789	0.861	0.727
CutPaste	0.864	0.900	0.851	0.907	0.773	0.671	0.653	0.683
DRAEM	0.954	0.912	0.869	0.897	0.810	0.760	0.726	0.693
FastFlow	0.885	0.867	0.854	0.855	0.836	0.725	0.725	0.691
FAVAE	0.768	0.801	0.798	0.814	0.536	0.476	0.482	0.525
IGD	0.805	0.801	0.782	0.790	0.797	0.786	0.789	0.756
PaDiM	0.890	0.907	0.899	0.906	0.675	0.580	0.626	0.608
PatchCore	0.990	0.986	0.975	0.980	0.857	0.790	0.782	0.763
RD4AD	0.989	0.984	0.975	0.983	0.909	0.837	0.826	0.824
SPADE	0.854	0.861	0.855	0.859	0.784	0.728	0.737	0.719
STPM	0.909	0.877	0.892	0.915	0.862	0.830	0.848	0.809

**Discussions.** Based on the statistical findings presented in Table X, it has been discovered that feature embedding-based methods are more effective than IGD when dealing with limited noise levels ( $\leq 0.15$ ). In order to identify the cause, we

have conducted a thorough investigation into the representative feature-embedding based method, PatchCore [60]. During the training phase, the objective is to establish a memory bank that stores neighborhood-aware features from all normal samples. The algorithm used to construct the feature memory is detailed in Algorithm 1.

#### Algorithm 1: PatchCore Pipeline

**Input :** ImageNet pretrained  $\phi$ , all normal samples  $\mathcal{X}_N$   
patch feature extractor  $\mathcal{P}$ , memory size target  $l$ ,  
random linear projection  $\psi$ .

**Output:** Patch-level augmented memory bank  $\mathcal{M}$ .

- 1  $\mathcal{M} \leftarrow \{\}$ ;
- 2 **for**  $x_i \in \mathcal{X}_N$  **do**
- 3    $\mathcal{M} \leftarrow \mathcal{M} \cup \mathcal{P}(\phi(x_i))$ ;
- 4 **end for**
- 5  $\mathcal{M}_C \leftarrow \{\}$  // Apply coreset sampling for memory bank
- 6 **for**  $i \in [0, \dots, l-1]$  **do**
- 7    $m_i \leftarrow \arg \max_{m \in \mathcal{M} - \mathcal{M}_C} \min_{n \in \mathcal{M}_C} \|\psi(m) - \psi(n)\|_2$ ;
- 8    $\mathcal{M}_C \leftarrow \mathcal{M}_C \cup \{m_i\}$ ;
- 9 **end for**
- 10  $\mathcal{M} \leftarrow \mathcal{M}_C$ .

TABLE XI

IMAGE AUROC  $\uparrow$  OF PATCHCORE UNDER DIFFERENT NOISE RATIOS AND NEIGHBOURHOOD NUMBERS. THE BEST AND SECOND-BEST RESULTS ARE MARKED IN RED AND BLUE, RESPECTIVELY.

Noise Ratio	Neighbour Number				
	1 (No Re-weighting)	2	3	6	9
0.05	0.990	0.988	0.990	0.987	0.990
0.1	0.986	0.989	0.986	0.984	0.983
0.15	0.975	0.983	0.979	0.986	0.984
0.2	0.980	0.982	0.976	0.986	0.982

By default, WideResNet-50 [87] is set as a feature extraction model. Coreset sampling [66] for memory banks aims to balance the size of memory banks with IAD performance. In inference, the test image will be predicted as an anomaly if at least one patch is anomalous, and pixel-level anomaly segmentation will be computed via the score of each patch feature. In particular, with the normal patch feature bank  $\mathcal{M}$ , the image-level anomaly score  $s$  for the test image  $x^{test}$  is computed by the maximum score  $s^*$  between the test image's patch feature  $\mathcal{P}(x^{test})$  and its nearest neighbor  $m^*$  in  $\mathcal{M}$ :

$$m^* = \arg \max_{m^{test} \in \mathcal{P}(x^{test})} \arg \min_{m \in \mathcal{M}} \|m^{test} - m\|_2, \quad (1)$$

TABLE XII

PERFORMANCE IN TERMS OF FM ON THE CONTINUAL SETTING. THE BEST AND SECOND-BEST RESULTS ARE MARKED IN RED AND BLUE, RESPECTIVELY.

Dataset	MVTec AD					MPDD				
	Image		Pixel			Image		Pixel		
Method	AUC↑ / FM↓	AP↑ / FM↓	AUC↑ / FM↓	AP↑ / FM↓	PRO↑ / FM↓	AUC↑ / FM↓	AP↑ / FM↓	AUC↑ / FM↓	AP↑ / FM↓	PRO↑ / FM↓
PatchCore	<b>0.919 / 0.003</b>	<b>0.971 / 0.001</b>	<b>0.944 / 0.002</b>	<b>0.481 / 0.005</b>	<b>0.847 / 0.001</b>	<b>0.786 / 0.015</b>	<b>0.851 / 0.021</b>	<b>0.963 / 0</b>	<b>0.358 / 0.0004</b>	<b>0.838 / 0.0001</b>
CFA	<b>0.623</b> / 0.361	<b>0.813</b> / 0.181	<b>0.753</b> / 0.217	<b>0.176</b> / 0.359	0.535 / 0.363	0.506 / 0.415	0.609 / 0.307	0.818 / 0.131	0.116 / 0.164	0.557 / 0.300
SPADE	0.571 / 0.284	0.781 / 0.159	0.746 / 0.208	0.151 / 0.319	<b>0.570</b> / 0.324	0.412 / 0.396	0.576 / 0.259	<b>0.912 / 0.069</b>	0.139 / 0.202	<b>0.732</b> / <b>0.193</b>
PaDiM	0.545 / 0.368	0.767 / 0.192	0.697 / 0.269	0.086 / 0.366	0.441 / 0.472	0.461 / 0.262	0.593 / 0.195	0.841 / 0.116	0.053 / 0.106	0.529 / 0.332
RD4AD	0.596 / 0.392	0.800 / 0.194	<b>0.753</b> / 0.222	0.143 / 0.425	0.531 / 0.401	0.646 / 0.344	<b>0.833</b> / 0.162	0.684 / 0.300	<b>0.158</b> / 0.407	0.532 / 0.414
STPM	0.576 / 0.324	0.786 / 0.163	0.625 / 0.277	0.109 / 0.352	0.322 / 0.446	0.499 / 0.339	0.617 / 0.267	0.328 / 0.648	0.099 / 0.217	0.217 / 0.701
CutPaste	0.312 / 0.509	0.650 / 0.270	–	–	–	<b>0.665 / 0.045</b>	0.724 / <b>0.061</b>	–	–	–
CSFlow	0.538 / 0.426	0.762 / 0.224	–	–	–	0.632 / 0.343	0.692 / 0.290	–	–	–
FastFlow	0.512 / 0.279	0.713 / 0.154	0.519 / 0.380	0.004 / 0.214	0.152 / 0.562	0.542 / 0.272	0.643 / 0.173	0.269 / 0.506	0.015 / <b>0.071</b>	0.061 / 0.448
FAVAE	0.547 / <b>0.101</b>	0.772 / <b>0.055</b>	0.673 / <b>0.107</b>	0.082 / <b>0.082</b>	0.390 / <b>0.157</b>	0.581 / 0.183	0.792 / 0.099	0.636 / 0.197	0.098 / 0.168	0.365 / 0.267
DNE	0.537 / 0.299	0.533 / 0.293	–	–	–	0.413 / 0.394	0.362 / 0.428	–	–	–

TABLE XIII

BENCHMARK OF THE REPRESENTATIVE VANILLA IAD ALGORITHMS IN IM-IAD SETTING, INCLUDING FEW-SHOT, NOISY LABEL, CONTINUAL LEARNING. THE BEST AND SECOND-BEST RESULTS ARE MARKED IN RED AND BLUE, RESPECTIVELY.

Dataset		MVTec AD					MPDD				
Metric	Method	Vanilla	Noisy-0.15	Few-shot-8	Continual	Mean	Vanilla	Noisy-0.15	Few-shot-8	Continual	Mean
Image AUC ↑	CFA	0.981	0.949	0.923	0.623	0.869	0.923	0.839	0.694	0.506	0.740
	CSFlow	0.952	0.904	0.845	0.539	0.810	0.973	0.861	0.741	0.633	0.802
	CutPaste	0.918	0.851	0.705	0.312	0.696	0.771	0.653	0.577	0.665	0.667
	DRAEM	0.981	0.869	0.883	0.595	0.832	0.941	0.726	0.773	0.440	0.720
	FastFlow	0.905	0.854	0.801	0.512	0.768	0.887	0.725	0.719	0.543	0.718
	FAVAE	0.793	0.798	0.690	0.547	0.707	0.570	0.482	0.390	0.582	0.506
	PaDiM	0.908	0.899	0.776	0.545	0.782	0.706	0.626	0.560	0.461	0.588
	PatchCore	0.992	0.975	0.864	0.919	0.938	0.948	0.782	0.694	0.787	0.803
	RD4AD	0.986	0.975	0.903	0.596	0.865	0.927	0.826	0.699	0.646	0.775
	SPADE	0.854	0.855	0.781	0.571	0.765	0.784	0.737	0.594	0.412	0.632
STPM	0.924	0.892	0.880	0.576	0.818	0.876	0.848	0.792	0.499	0.754	
Pixel AP ↑	CFA	0.538	0.394	0.513	0.177	0.406	0.283	0.212	0.269	0.117	0.220
	CSFlow	—	—	—	—	—	—	—	—	—	—
	CutPaste	—	—	—	—	—	—	—	—	—	—
	DRAEM	0.689	0.337	0.442	0.098	0.391	0.288	0.174	0.286	0.131	0.220
	FastFlow	0.398	0.313	0.279	0.044	0.259	0.115	0.055	0.116	0.015	0.075
	FAVAE	0.307	0.319	0.223	0.083	0.233	0.088	0.080	0.073	0.099	0.085
	PaDiM	0.452	0.454	0.362	0.086	0.339	0.155	0.136	0.102	0.053	0.112
	PatchCore	0.561	0.500	0.440	0.481	0.496	0.432	0.254	0.240	0.358	0.321
	RD4AD	0.580	0.532	0.490	0.143	0.436	0.455	0.374	0.245	0.158	0.308
	SPADE	0.471	0.410	0.405	0.151	0.359	0.342	0.309	0.261	0.140	0.263
STPM	0.518	0.465	0.494	0.110	0.354	0.354	0.309	0.321	0.100	0.271	

$$s^* = \|m^{test} - m^*\|_2. \quad (2)$$

To enhance model robustness, PatchCore employs the importance re-weighting [47] to tune the anomaly score  $s$ .

$$s = \left(1 - \frac{\exp \|m^{test,*} - m^*\|_2}{\sum_{m \in \mathcal{N}_b(m^*)} \exp \|m^{test,*} - m^*\|_2}\right) \cdot s^*, \quad (3)$$

where  $\mathcal{N}_b(m^*)$  denotes  $b$  nearest patch-features in  $\mathcal{M}$  for test patch-feature  $m^*$ . Furthermore, we conducted ablation studies to verify the effect of re-weighting. The statistical result of Table XI shows that re-weighting improves the resilience of IAD algorithms when the noise ratio is larger than 10%.

**Challenges.** The selection of samples is essential to improve IAD robustness. From Table X, it is clear that robust unsupervised IAD algorithms can be improved. We believe that sample selection has great potential in the future, as it can be seamlessly integrated with current IAD methods. For example, Song *et al.* [69] create a discriminative network to distinguish true-labeled cases from noisy training data, *i.e.*, one for sample selection and the other for anomalous detection.

#### F. Memory Bank-based Methods for Continual IAD

**Settings.** We benchmark the vanilla methods and the continual baseline IAD method, DNE [45] according to the continual setting in Sec. III-A-5.

**Discussions.** Table XII indicates that memory bank-based methods provide satisfactory performance to overcome the catastrophic forgetting phenomenon among all unsupervised IAD, although these methods are not specifically proposed for continual IAD settings. The main idea behind this is that the replay method is perfectly appropriate for memory-based IAD algorithms. Memory bank-based methods can easily add new memory to reduce forgetting when learning new tasks. Ideally, the memory bank should work for the test mechanism. During the test, the memory bank-based method can easily combine the nearest-mean classifier to locate the nearest memory when the test sample is provided.

**Challenges.** In the continual IAD setting, limiting the size of the memory database and minimizing interference from previous tasks is of utmost importance. When learning new tasks, simply adding more memory significantly slows down the inference time and increases storage usage. For a fixed

storage need, we suggest using the storage sampling [59] to limit the number of instances that can be stored. Furthermore, the memory of the new task may overlap with the memory of the previous task, causing IAD performance to decrease. Consequently, the main challenge is to design a new constraint optimization loss function to avoid task interference.

### G. Uniform View on IM-IAD

**Settings.** We benchmark vanilla algorithms in a uniform IM-IAD setting, including few-shot, noisy, and continual settings, which are described in Sec. III-A.

**Discussions.** Table XIII shows that PatchCore achieves the SOTA result in our IM-IAD setting. However, as shown in Fig. 2, PatchCore is inferior to other IAD algorithms in terms of GPU memory usage and inference time, making its use challenging in real scenarios. Furthermore, maintaining the size of the memory bank is a critical issue for realistic deployment if the number of object classes exceeds 100. Therefore, to bridge the gap between academic research and industry, there are still opportunities for IAD algorithms.

**Challenges.** Multi-objective neural architecture search (NAS) is a considerably promising direction for IAD in finding the optimal trade-off architecture. If the IAD model can be applied in practice, many objectives need to be satisfied, like fast speed of inference, low memory usage, and continual learning ability. Because the memory capacity of edge devices used in production lines is heavily restricted. Moreover, most IAD methods cannot predict the arrival of new test samples instantly when test samples are sequentially streamed on the product line.

## V. CONCLUSION

We introduce IM-IAD in this paper, thus far the most complete industrial manufacturing-based IAD benchmark with 19 algorithms, 7 datasets, and 5 settings. We have gained insights into the importance of partial labels for fully supervised learning, the influence of noise ratio in noisy settings, the design principles for continual learning, and the important role of global features for logical anomalies. On top of these, we present several intriguing future lines for industrial IAD.

## ACKNOWLEDGMENTS

This work is partially supported by the National Key R&D Program of China (Grant NO. 2022YFF1202903) and the National Natural Science Foundation of China (Grant NO. 62122035, 61972188, and 62206122).

## REFERENCES

- [1] Kilian Batzner, Lars Heckler, and Rebecca König. Efficientad: Accurate visual anomaly detection at millisecond-level latencies. *ArXiv*, abs/2303.14535, 2023.
- [2] Paul Bergmann, Kilian Batzner, Michael Fauser, David Sattlegger, and Carsten Steger. The mvtec anomaly detection dataset: a comprehensive real-world dataset for unsupervised anomaly detection. *International Journal of Computer Vision*, 129(4):1038–1059, 2021.
- [3] Paul Bergmann, Kilian Batzner, Michael Fauser, David Sattlegger, and Carsten Steger. Beyond dents and scratches: Logical constraints in unsupervised anomaly detection and localization. *International Journal of Computer Vision*, 130(4):947–969, 2022.
- [4] Paul Bergmann, Michael Fauser, David Sattlegger, and Carsten Steger. Mvtec ad — a comprehensive real-world dataset for unsupervised anomaly detection. *2019 IEEE/CVF Conference on Computer Vision and Pattern Recognition (CVPR)*, pages 9584–9592, 2019.
- [5] Paul Bergmann, Michael Fauser, David Sattlegger, and Carsten Steger. Uninformed students: Student-teacher anomaly detection with discriminative latent embeddings. In *Proceedings of the IEEE/CVF Conference on Computer Vision and Pattern Recognition*, pages 4183–4192, 2020.
- [6] Paul Bergmann, Xin Jin, David Sattlegger, and Carsten Steger. The mvtec 3d-ad dataset for unsupervised 3d anomaly detection and localization. *arXiv preprint arXiv:2112.09045*, 2021.
- [7] Paul Bergmann, Sindy Löwe, Michael Fauser, David Sattlegger, and Carsten Steger. Improving unsupervised defect segmentation by applying structural similarity to autoencoders. *arXiv preprint arXiv:1807.02011*, 2018.
- [8] Luca Bonfiglioli, Marco Toschi, Davide Silvestri, Nicola Fioraio, and Daniele De Gregorio. The eyecandies dataset for unsupervised multimodal anomaly detection and localization. In *Asian Conference on Computer Vision*, 2022.
- [9] Yunkang Cao, Xiaohao Xu, Chen Sun, Yuqi Cheng, Zongwei Du, Liang Gao, and Weiming Shen. Segment any anomaly without training via hybrid prompt regularization. *arXiv preprint arXiv:2305.10724*, 2023.
- [10] Arslan Chaudhry, Puneet Kumar Dokania, Thalaiyasingam Ajanthan, and Philip H. S. Torr. Riemannian walk for incremental learning: Understanding forgetting and intransigence. *ArXiv*, abs/1801.10112, 2018.
- [11] Yuanhong Chen, Yu Tian, Guansong Pang, and G. Carneiro. Deep one-class classification via interpolated gaussian descriptor. In *AAAI*, 2022.
- [12] Yuanhong Chen, Yu Tian, Guansong Pang, and Gustavo Carneiro. Deep one-class classification via interpolated gaussian descriptor. *Proceedings of the AAAI Conference on Artificial Intelligence*, 36(1):383–392, 2022.
- [13] Z. Chen, Yanwei Fu, Kaiyu Chen, and Yu-Gang Jiang. Image block augmentation for one-shot learning. In *AAAI Conference on Artificial Intelligence*, 2019.
- [14] Wen-Hsuan Chu and Kris M Kitani. Neural batch sampling with reinforcement learning for semi-supervised anomaly detection. In *European conference on computer vision*, pages 751–766. Springer, 2020.
- [15] Niv Cohen and Yedid Hoshen. Sub-image anomaly detection with deep pyramid correspondences. *arXiv preprint arXiv:2005.02357*, 2020.
- [16] Anne-Sophie Collin and Christophe De Vleeschouwer. Improved anomaly detection by training an autoencoder with skip connections on images corrupted with stain-shaped noise. In *2020 25th International Conference on Pattern Recognition (ICPR)*, pages 7915–7922. IEEE, 2021.
- [17] Antoine Cordier, Benjamin Missaoui, and Pierre Gutierrez. Data refinement for fully unsupervised visual inspection using pre-trained networks. *arXiv preprint arXiv:2202.12759*, 2022.
- [18] German chapter of the IAPR (International Association for Pattern Recognition) DAGM (Deutsche Arbeitsgemeinschaft für Mustererkennung e.V. and the GNSS (German Chapter of the European Neural Network Society). Dagm dataset. <http://www.thisisurl/>, 2000.
- [19] Puck de Haan and Sindy Löwe. Contrastive predictive coding for anomaly detection. *arXiv preprint arXiv:2107.07820*, 2021.
- [20] Thomas Defard, Aleksandr Setkov, Angelique Loesch, and Romaric Audigier. Padim: a patch distribution modeling framework for anomaly detection and localization. In *International Conference on Pattern Recognition*, pages 475–489. Springer, 2021.
- [21] David Dehaene and Pierre Eline. Anomaly localization by modeling perceptual features. *ArXiv*, abs/2008.05369, 2020.
- [22] David Dehaene, Oriel Frigo, Sébastien Combexelle, and Pierre Eline. Iterative energy-based projection on a normal data manifold for anomaly localization. In *International Conference on Learning Representations*, 2019.
- [23] Hanqiu Deng and Xingyu Li. Anomaly detection via reverse distillation from one-class embedding. *ArXiv*, abs/2201.10703, 2022.
- [24] Jan Diers and Christian Pigorsch. A survey of methods for automated quality control based on images. *International Journal of Computer Vision*, 131:2553 – 2581, 2023.
- [25] Choubo Ding, Guansong Pang, and Chunhua Shen. Catching both gray and black swans: Open-set supervised anomaly detection. In *Proceedings of the IEEE/CVF Conference on Computer Vision and Pattern Recognition*, pages 7388–7398, 2022.
- [26] Alexey Dosovitskiy, Lucas Beyer, Alexander Kolesnikov, Dirk Weissenborn, Xiaohua Zhai, Thomas Unterthiner, Mostafa Dehghani, Matthias Minderer, Georg Heigold, Sylvain Gelly, Jakob Uszkoreit, and Neil Houlsby. An image is worth 16x16 words: Transformers for image recognition at scale. *ArXiv*, abs/2010.11929, 2020.
- [27] Denis Gudovskiy, Shun Ishizaka, and Kazuki Kozuka. Cflow-ad: Real-time unsupervised anomaly detection with localization via conditional

- normalizing flows. In *Proceedings of the IEEE/CVF Winter Conference on Applications of Computer Vision*, pages 98–107, 2022.
- [28] Songqiao Han, Xiyang Hu, Hailiang Huang, Mingqi Jiang, and Yue Zhao. Adbench: Anomaly detection benchmark. *ArXiv*, abs/2206.09426, 2022.
- [29] Jinlei Hou, Yingying Zhang, Qiaoyong Zhong, Di Xie, Shiliang Pu, and Hong Zhou. Divide-and-assemble: Learning block-wise memory for unsupervised anomaly detection. In *Proceedings of the IEEE/CVF International Conference on Computer Vision*, pages 8791–8800, 2021.
- [30] Chuanfei Hu, Kai Chen, and Hang Shao. A semantic-enhanced method based on deep svdd for pixel-wise anomaly detection. In *2021 IEEE International Conference on Multimedia and Expo (ICME)*, pages 1–6. IEEE, 2021.
- [31] Chaoqin Huang, Haoyan Guan, Aofan Jiang, Ya Zhang, Michael Spratling, and Yan-Feng Wang. Registration based few-shot anomaly detection. *arXiv preprint arXiv:2207.07361*, 2022.
- [32] Yibin Huang, Congying Qiu, and Kui Yuan. Surface defect saliency of magnetic tile. *The Visual Computer*, 36(1):85–96, 2020.
- [33] Stepan Jezek, Martin Jonak, Radim Burget, Pavel Dvorak, and Milos Skotak. Deep learning-based defect detection of metal parts: evaluating current methods in complex conditions. In *2021 13th International Congress on Ultra Modern Telecommunications and Control Systems and Workshops (ICUMT)*, pages 66–71. IEEE, 2021.
- [34] Jieli Jiang, Jiale Zhu, Muhammad Bilal, Yan Cui, Neeraj Kumar, Ruihan Dou, Feng Su, and Xiaolong Xu. Masked swin transformer unet for industrial anomaly detection. *IEEE Transactions on Industrial Informatics*, 2022.
- [35] Xi Jiang, Jianlin Liu, Jinbao Wang, Qiang Nie, Kai Wu, Yong Liu, Chengjie Wang, and Feng Zheng. Softpatch: Unsupervised anomaly detection with noisy data. *Advances in Neural Information Processing Systems*, 35:15433–15445, 2022.
- [36] Ammar Mansoor Kamooona, Amirali Khodadadian Gostar, Alireza Bab-Hadiashar, and Reza Hoseinnezhad. Anomaly detection of defect using energy of point pattern features within random finite set framework. *arXiv preprint arXiv:2108.12159*, 2021.
- [37] Jin-Hwa Kim, Do-Hyeong Kim, Saehoon Yi, and Taehoon Lee. Semi-orthogonal embedding for efficient unsupervised anomaly segmentation. *arXiv preprint arXiv:2105.14737*, 2021.
- [38] Alexander Kirillov, Eric Mintun, Nikhila Ravi, Hanzi Mao, Chloe Rolland, Laura Gustafson, Tete Xiao, Spencer Whitehead, Alexander C Berg, Wan-Yen Lo, et al. Segment anything. *arXiv preprint arXiv:2304.02643*, 2023.
- [39] Ivan Kobzyev, Simon Prince, and Marcus A. Brubaker. Normalizing flows: Introduction and ideas. *ArXiv*, abs/1908.09257, 2019.
- [40] Sungwook Lee, Seunghyun Lee, and Byung Cheol Song. Cfa: Coupled-hypersphere-based feature adaptation for target-oriented anomaly localization. *arXiv preprint arXiv:2206.04325*, 2022.
- [41] Chao Li, Jun Li, Yafei Li, Lingmin He, Xiaokang Fu, and Jingjing Chen. Fabric defect detection in textile manufacturing: a survey of the state of the art. *Security and Communication Networks*, 2021:1–13, 2021.
- [42] Chun-Liang Li, Kihyuk Sohn, Jinsung Yoon, and Tomas Pfister. Cut-paste: Self-supervised learning for anomaly detection and localization. In *Proceedings of the IEEE/CVF Conference on Computer Vision and Pattern Recognition*, pages 9664–9674, 2021.
- [43] Hanxi Li, Jingqi Wu, Hao Chen, Mingwen Wang, and Chunhua Shen. Efficient anomaly detection with budget annotation using semi-supervised residual transformer. *arXiv preprint arXiv:2306.03492*, 2023.
- [44] Ning Li, Kaitao Jiang, Zhiheng Ma, Xing Wei, Xiaopeng Hong, and Yihong Gong. Anomaly detection via self-organizing map. In *2021 IEEE International Conference on Image Processing (ICIP)*, pages 974–978. IEEE, 2021.
- [45] Wujin Li, Jiawei Zhan, Jinbao Wang, Bizhong Xia, Bin-Bin Gao, Jun Liu, Chengjie Wang, and Feng Zheng. Towards continual adaptation in industrial anomaly detection. In *Proceedings of the 30th ACM International Conference on Multimedia*, pages 2871–2880, 2022.
- [46] Jiaqi Liu, Guoyang Xie, Jingbao Wang, Shangnian Li, Chengjie Wang, Feng Zheng, and Yaochu Jin. Deep industrial image anomaly detection: A survey. *arXiv preprint arXiv:2301.11514*, 2, 2023.
- [47] Tongliang Liu and Dacheng Tao. Classification with noisy labels by importance reweighting. *IEEE Transactions on Pattern Analysis and Machine Intelligence*, 38:447–461, 2014.
- [48] Wenqian Liu, Runze Li, Meng Zheng, Srikrishna Karanam, Ziyang Wu, Bir Bhanu, Richard J Radke, and Octavia Camps. Towards visually explaining variational autoencoders. In *Proceedings of the IEEE/CVF Conference on Computer Vision and Pattern Recognition*, pages 8642–8651, 2020.
- [49] Zhikang Liu, Yiming Zhou, Yuansheng Xu, and Zilei Wang. Simplenet: A simple network for image anomaly detection and localization. *2023 IEEE/CVF Conference on Computer Vision and Pattern Recognition (CVPR)*, pages 20402–20411, 2023.
- [50] Philipp Liznerski, Lukas Ruff, Robert A Vandermeulen, Billy Joe Franks, Marius Kloft, and Klaus Robert Muller. Explainable deep one-class classification. In *International Conference on Learning Representations*, 2020.
- [51] Fabio Valerio Massoli, Fabrizio Falchi, Alperen Kantarci, Şeymanur Akti, Hazim Kemal Ekenel, and Giuseppe Amato. Mocca: Multilayer one-class classification for anomaly detection. *IEEE Transactions on Neural Networks and Learning Systems*, 2021.
- [52] Pankaj Mishra, Riccardo Verk, Daniele Fornasier, Claudio Picciarelli, and Gian Luca Foresti. Vt-adl: A vision transformer network for image anomaly detection and localization. In *2021 IEEE 30th International Symposium on Industrial Electronics (ISIE)*, pages 01–06. IEEE, 2021.
- [53] Renkun Ni, Micah Goldblum, Amr Sharaf, Kezhi Kong, and Tom Goldstein. Data augmentation for meta-learning. In *International Conference on Machine Learning*, 2020.
- [54] Guansong Pang, Choubo Ding, Chunhua Shen, and Anton van den Hengel. Explainable deep few-shot anomaly detection with deviation networks. *arXiv preprint arXiv:2108.00462*, 2021.
- [55] Jonathan Pirnay and Keng Chai. Inpainting transformer for anomaly detection. In *International Conference on Image Analysis and Processing*, pages 394–406. Springer, 2022.
- [56] Chen Qiu, Aodong Li, Marius Kloft, Maja Rudolph, and Stephan Mandt. Latent outlier exposure for anomaly detection with contaminated data. *arXiv preprint arXiv:2202.08088*, 2022.
- [57] Punit Rathore, Dheeraj Kumar, James C. Bezdek, Sutharshan Rajasegarar, and Marimuthu Swami Palaniswami. Visual structural assessment and anomaly detection for high-velocity data streams. *IEEE Transactions on Cybernetics*, 51:5979–5992, 2020.
- [58] Tal Reiss, Niv Cohen, Liron Bergman, and Yedid Hoshen. Panda: Adapting pretrained features for anomaly detection and segmentation. *2021 IEEE/CVF Conference on Computer Vision and Pattern Recognition (CVPR)*, pages 2805–2813, 2021.
- [59] David Rolnick, Arun Ahuja, Jonathan Schwarz, Timothy P. Lillicrap, and Greg Wayne. Experience replay for continual learning. In *NeurIPS*, 2019.
- [60] Karsten Roth, Latha Pemula, Joaquin Zepeda, Bernhard Schölkopf, Thomas Brox, and Peter Gehler. Towards total recall in industrial anomaly detection. In *Proceedings of the IEEE/CVF Conference on Computer Vision and Pattern Recognition*, pages 14318–14328, 2022.
- [61] Marco Rudolph, Bastian Wandt, and Bodo Rosenhahn. Same same but different: Semi-supervised defect detection with normalizing flows. In *Proceedings of the IEEE/CVF winter conference on applications of computer vision*, pages 1907–1916, 2021.
- [62] Marco Rudolph, Tom Wehrbein, Bodo Rosenhahn, and Bastian Wandt. Fully convolutional cross-scale-flows for image-based defect detection. In *Proceedings of the IEEE/CVF Winter Conference on Applications of Computer Vision*, pages 1088–1097, 2022.
- [63] Mohammadreza Salehi, Niousha Sadjadi, Soroosh Baselizadeh, Mohammad H Rohban, and Hamid R Rabiee. Multiresolution knowledge distillation for anomaly detection. In *Proceedings of the IEEE/CVF conference on computer vision and pattern recognition*, pages 14902–14912, 2021.
- [64] Daniel Sauter, Anna Schmitz, Fulya Dikici, Hermann Baumgartl, and Ricardo Buettner. Defect detection of metal nuts applying convolutional neural networks. In *2021 IEEE 45th Annual Computers, Software, and Applications Conference (COMPSAC)*, pages 248–257. IEEE, 2021.
- [65] Hannah M Schlüter, Jeremy Tan, Benjamin Hou, and Bernhard Kainz. Self-supervised out-of-distribution detection and localization with natural synthetic anomalies (nsa). *arXiv preprint arXiv:2109.15222*, 2021.
- [66] Ozan Sener and Silvio Savarese. Active learning for convolutional neural networks: A core-set approach. *arXiv: Machine Learning*, 2018.
- [67] Shelly Sheynin, Sagie Benaim, and Lior Wolf. A hierarchical transformation-discriminating generative model for few shot anomaly detection. In *Proceedings of the IEEE/CVF International Conference on Computer Vision*, pages 8495–8504, 2021.
- [68] Kihyuk Sohn, Chun-Liang Li, Jinsung Yoon, Minho Jin, and Tomas Pfister. Learning and evaluating representations for deep one-class classification. In *International Conference on Learning Representations*, 2020.
- [69] Hwanjun Song, Minseok Kim, and Jae-Gil Lee. Selfie: Refurbishing unclean samples for robust deep learning. In *International Conference on Machine Learning*, 2019.
- [70] Daniel Stanley Tan, Yi-Chun Chen, Trista Pei-Chun Chen, and Wei-Chao Chen. Trustmae: A noise-resilient defect classification framework using memory-augmented auto-encoders with trust regions. In *Proceedings of the IEEE/CVF winter conference on applications of computer vision*, pages 276–285, 2021.
- [71] Xian Tao, Xinyi Gong, Xin Yu Zhang, Shaohua Yan, and Chandranath



- Adak. Deep learning for unsupervised anomaly localization in industrial images: A survey. *IEEE Transactions on Instrumentation and Measurement*, 71:1–21, 2022.
- [72] Colin SC Tsang, Henry YT Ngan, and Grantham KH Pang. Fabric inspection based on the elo rating method. *Pattern Recognition*, 51:378–394, 2016.
- [73] Shashanka Venkataramanan, Kuan-Chuan Peng, Rajat Vikram Singh, and Abhijit Mahalanobis. Attention guided anomaly localization in images. In *European Conference on Computer Vision*, pages 485–503. Springer, 2020.
- [74] Guodong Wang, Shumin Han, Errui Ding, and Di Huang. Student-teacher feature pyramid matching for anomaly detection. In *BMVC*, 2021.
- [75] Hengli Wang, Rui Fan, Yuxiang Sun, and Ming Liu. Dynamic fusion module evolves drivable area and road anomaly detection: A benchmark and algorithms. *IEEE transactions on cybernetics*, 52(10):10750–10760, 2021.
- [76] Min Wang, Donghua Zhou, and Maoyin Chen. Hybrid variable monitoring mixture model for anomaly detection in industrial processes. *IEEE transactions on cybernetics*, PP, 2022.
- [77] Guoyang Xie, Jinbao Wang, Jiaqi Liu, Yaochu Jin, and Feng Zheng. Pushing the limits of fewshot anomaly detection in industry vision: Graphcore. In *The Eleventh International Conference on Learning Representations*, 2023.
- [78] Shinji Yamada and Kazuhiro Hotta. Reconstruction student with attention for student-teacher pyramid matching. *arXiv preprint arXiv:2111.15376*, 2021.
- [79] Xudong Yan, Huaidong Zhang, Xuemiao Xu, Xiaowei Hu, and Pheng-Ann Heng. Learning semantic context from normal samples for unsupervised anomaly detection. In *Proceedings of the AAAI Conference on Artificial Intelligence*, volume 35, pages 3110–3118, 2021.
- [80] Yi Yan, Deming Wang, Guangliang Zhou, and Qijun Chen. Unsupervised anomaly segmentation via multilevel image reconstruction and adaptive attention-level transition. *IEEE Transactions on Instrumentation and Measurement*, 70:1–12, 2021.
- [81] Jie Yang, Yong Shi, and Zhiqian Qi. Dfr: Deep feature reconstruction for unsupervised anomaly segmentation. *arXiv preprint arXiv:2012.07122*, 2020.
- [82] Xincheng Yao, Ruqi Li, Jing Zhang, Jun Sun, and Chongyang Zhang. Explicit boundary guided semi-push-pull contrastive learning for supervised anomaly detection. In *Proceedings of the IEEE/CVF Conference on Computer Vision and Pattern Recognition*, pages 24490–24499, 2023.
- [83] Jihun Yi and Sungroh Yoon. Patch svdd: Patch-level svdd for anomaly detection and segmentation. In *Proceedings of the Asian Conference on Computer Vision*, 2020.
- [84] Yong-Ho Yoo, Ue-Hwan Kim, and Jong hwan Kim. Convolutional recurrent reconstructive network for spatiotemporal anomaly detection in solder paste inspection. *IEEE Transactions on Cybernetics*, 52:4688–4700, 2019.
- [85] Jinsung Yoon, Kihyuk Sohn, Chun-Liang Li, Serkan O Arik, Chen-Yu Lee, and Tomas Pfister. Self-supervise, refine, repeat: Improving unsupervised anomaly detection. 2021.
- [86] Jiawei Yu, Ye Zheng, Xiang Wang, Wei Li, Yushuang Wu, Rui Zhao, and Liwei Wu. Fastflow: Unsupervised anomaly detection and localization via 2d normalizing flows. *arXiv preprint arXiv:2111.07677*, 2021.
- [87] Sergey Zagoruyko and Nikos Komodakis. Wide residual networks. In *Proceedings of the British Machine Vision Conference 2016*. British Machine Vision Association, 2016.
- [88] Vitjan Zavrtanik, Matej Kristan, and Danijel Skočaj. Draem-a discriminatively trained reconstruction embedding for surface anomaly detection. In *Proceedings of the IEEE/CVF International Conference on Computer Vision*, pages 8330–8339, 2021.
- [89] Vitjan Zavrtanik, Matej Kristan, and Danijel Skočaj. Reconstruction by inpainting for visual anomaly detection. *Pattern Recognition*, 112:107706, 2021.
- [90] Vitjan Zavrtanik, Matej Kristan, and Danijel Skočaj. Dsr—a dual subspace re-projection network for surface anomaly detection. *arXiv preprint arXiv:2208.01521*, 2022.
- [91] Hui Zhang, Zuxuan Wu, Zheng Wang, Zhineng Chen, and Yu-Gang Jiang. Prototypical residual networks for anomaly detection and localization. In *Proceedings of the IEEE/CVF Conference on Computer Vision and Pattern Recognition*, pages 16281–16291, 2023.
- [92] Jian Zhang, Ge Yang, Miaoju Ban, and Runwei Ding. Pku-goodsad: A supermarket goods dataset for unsupervised anomaly detection and segmentation. *arXiv preprint arXiv:2307.04956*, 2023.
- [93] Ye Zheng, Xiang Wang, Yu-Hang Qi, Wei Li, and Liwei Wu. Benchmarking unsupervised anomaly detection and localization. *ArXiv*, abs/2205.14852, 2022.
- [94] Yang Zou, Jongheon Jeong, Latha Pemula, Dongqing Zhang, and Onkar Dabeer. Spot-the-difference self-supervised pre-training for anomaly detection and segmentation. *arXiv preprint arXiv:2207.14315*, 2022.